



Dissect two-halo galactic conformity effect for central galaxies: The dependence of star formation activities on the large-scale environment

Kai Wang ¹★, Yingjie Peng^{2,1}† and Yangyao Chen ^{3,4}

¹Kavli Institute for Astronomy and Astrophysics, Peking University, Beijing 100871, China

²Department of Astronomy, School of Physics, Peking University, Beijing 100871, China

³School of Astronomy and Space Science, University of Science and Technology of China, Hefei 230026, China

⁴Key Laboratory for Research in Galaxies and Cosmology, Department of Astronomy, University of Science and Technology of China, Hefei, Anhui 230026, China

Last updated 2020 May 22; in original form 2018 September 5

ABSTRACT

We investigate the two-halo galactic conformity effect for central galaxies, which is the spatial correlation of the star formation activities for central galaxies to several Mpcs, by studying the dependence of the star formation activities of central galaxies on their large-scale structure in our local Universe using the SDSS data. Here we adopt a novel environment metric using only central galaxies quantified by the distance to the n -th nearest central galaxy. This metric measures the environment within an aperture from ~ 1 Mpc to $\gtrsim 10$ Mpc, with a median value of ~ 4 Mpc. We found that two kinds of conformity effects in our local Universe. The first one is that low-mass central galaxies are more quenched in high-density regions, and we found that this effect mainly comes from low-mass centrals that are close to a more massive halo. A similar trend is also found in the IllustrisTNG simulation, which can be entirely explained by backplash galaxies. The second conformity effect is that massive central galaxies in low-density regions are more star-forming. This population of galaxies also possesses a higher fraction of spiral morphology and lower central stellar velocity dispersion, suggesting that their low quiescent fraction is due to less-frequent major merger events experienced in the low-density regions, and as a consequence, less-massive bulges and central black holes.

Key words: methods: statistical - galaxies: groups: general - dark matter - large-scale structure of Universe

1 INTRODUCTION

Observational data of galaxy surveys shows a strong bimodality in terms of galaxy properties, where one population is blue, star-forming, and spiral-like, while the other one is red, quiescent, and spheroidal-like (e.g. [Strateva et al. 2001](#); [Hogg et al. 2002](#); [Ellis et al. 2005](#); [Ball et al. 2006](#); [Baldry et al. 2006](#); [Peng et al. 2010](#)). Galaxies must be star-forming at first to accumulate their stellar mass before evolving into the quiescent population, where this transition is also known as the quenching process. There are many quenching mechanisms proposed in the literature, and they can be categorized into internal and external channels. The former includes the feedback effects from the accretion of central massive black holes (e.g. [Croton et al. 2006](#); [Fabian 2012](#)), the inefficient cooling for gas in massive halos ([Dekel & Birnboim 2006](#)), morphological quenching ([Martig et al. 2009](#); [Genzel et al. 2014](#); [Gensior et al. 2020](#)), and angular momentum quenching ([Renzini 2020](#); [Peng & Renzini 2020](#)). Meanwhile, the latter includes the strangulation effect (e.g. [Larson](#)

[et al. 1980](#); [Peng et al. 2015](#)), the harassment effect (e.g. [Moore et al. 1996](#); [Smith et al. 2010](#)), and the ram-pressure stripping effect ([Gunn & Gott 1972](#)). In addition, [Peng et al. \(2010\)](#) showed that the dependence of the quiescent fraction on stellar mass and local environment is empirically separable, suggesting that these two mechanisms, i.e. mass quenching and environment quenching, are affecting the star formation activities of galaxies independently (see also [Baldry et al. 2006](#)). Furthermore, [Peng et al. \(2012\)](#) found that the quiescent fraction of central galaxies primarily depends on stellar mass, while both mass quenching and environment quenching are affecting the evolution of satellite galaxies (see also [Wang et al. 2018](#)).

In addition, [Weinmann et al. \(2006\)](#) found that the star-forming activities of satellites also correlate with the star formation states of their central galaxies with both stellar mass and halo mass fixed. This effect is known as the one-halo conformity effect (see also [Knobel et al. 2015](#); [Treyer et al. 2018](#)). The robustness of this effect is still under debate since the halo mass calibration through the heuristic abundance matching method ignores their dependence on the colors/star-forming activities of central galaxies ([Mandelbaum](#)

★ e-mail: wkcosmology@gmail.com

† e-mail: yjpeng@pku.edu.cn

et al. 2016). Later, Kauffmann et al. (2013) found that the correlation between the star formation states of central galaxies and their neighboring galaxies extends to several Mpc, much larger than the virial radius of host halos. This effect is named the two-halo galactic conformity effect (see also Hearin et al. 2015, 2016; Sin et al. 2019; Ayromlou et al. 2022), which is the focus of this paper. It is noteworthy that similar conformity effects are also found for other properties of galaxies (e.g. Wang et al. 2015; Calderon et al. 2018; Otter et al. 2020) and for high- z galaxies (e.g. Hartley et al. 2015; Kawinwanichakij et al. 2016; Berti et al. 2017).

There are many mechanisms proposed in the literature to explain the two-halo conformity effect. Kauffmann (2015) proposed that gas is heated over large scales by the active galactic nuclei (AGN) feedback effect, since they found an excess number of massive galaxies around quiescent central galaxies, and these massive galaxies have higher probability to host radio-loud AGNs. Hearin et al. (2015) claimed that the conformity signal is a smoking gun of halo assembly bias, i.e. early-formed halos are more clustered, since they can reproduce the conformity signal in simulations assuming that central galaxies in early-formed halos are more quenched (see also Wang et al. 2023b). Based on the same philosophy, Hearin et al. (2016) found that the conformity signal can also be explained by correlating the star-forming activities of central galaxies with the accretion rate of their host halos, since the latter exhibits strong spatial correlation over several Mpcs. Alternatively, Zu & Mandelbaum (2018) showed that the conformity signal can be reproduced in a model that galaxy quenching is only determined by their stellar mass and host halo mass, and no super-halo-scale physical processes nor assembly bias is required. Recently, Ayromlou et al. (2022) found that the conformity effect may originate from the super-halo-scale ram-pressure stripping effect. The evidence is that the conformity signal emerges from the semi-analytical model of L-GALAXIES (Henriques et al. 2015, 2020) once a recipe that can strip gas from galaxies out of halo boundaries is introduced (Ayromlou et al. 2021).

The two-halo galactic conformity effect also manifests itself in the semi-analytical and hydrodynamical models of galaxy formation (Bray et al. 2016; Lacerna et al. 2018). Sun et al. (2018) showed that the two-halo galactic conformity effect is due to that the star formation activities of central galaxies have a dependence on their environment, and they found a similar signal in the semi-analytical model of Guo et al. (2011). Besides, Lacerna et al. (2022) found similar two-halo conformity signals in the semi-analytical model of SAG and the IllustrisTNG hydrodynamical simulation, and this signal can be eliminated once central galaxies in the vicinity of massive clusters are removed (Sin et al. 2017; Ayromlou et al. 2021).

The original definition of two-halo galactic conformity in Kauffmann et al. (2013) is the correlation between the star formation in central galaxies (primary galaxies), which are identified using the isolation criterion, and their neighbors (secondary galaxies) up to several Mpcs. This definition has several flaws. First, the isolation criterion can introduce fake signals by misidentifying satellite galaxies as centrals (Sin et al. 2017; Tinker et al. 2018a). Second, the secondary galaxies include both central and satellite galaxies, so that the one-halo and two-halo galactic conformity effects are mixed, which makes the result hard to interpret (Paranjape et al. 2015; Tinker et al. 2017, 2018b, see also § 4.3). Finally, the correlation between primary and secondary galaxies can be explained by either a causal relation between them, or a scenario that both kinds of galaxies are affected by a mediate property, or both. In order to alleviate the impact of these flaws and make the results interpretable, here we study the star formation of central galaxies, identified by

the halo-based group finding algorithm of Yang et al. (2007) (see also Yang et al. 2005; Lu et al. 2016; Lim et al. 2017; Wang et al. 2020; Yang et al. 2021; Li et al. 2022), and its dependence on the large-scale environment traced by central galaxies only. In the remaining content, we will refer to the dependence of the star formation activities of central galaxies on the large-scale environment as the two-halo conformity effect, unless specified otherwise.

This paper is organized as follows. § 2 introduces the galaxy sample from observation and simulation, as well as the calculation of our large-scale environment metric. The main results are presented in § 3, and the discussion is in § 4. And we will summarize in § 5. Throughout this paper, we are assuming a concordance Λ CDM cosmology with $H_0 = 100h$ km/s/Mpc, $h = 0.7$, $\Omega_\Lambda = 0.75$, and $\Omega_m = 0.25$.

2 DATA

2.1 Galaxy catalog

The sample used for this study is drawn from the Sloan Digital Sky Survey (SDSS) main galaxy sample (MGS), which is a magnitude-limited spectroscopic survey with $r < 17$ covering ~ 8000 deg² carried on the 2.5 meter wide-angle telescope at Apache Point Observatory (York et al. 2000; Blanton et al. 2005; Abazajian et al. 2009). The SDSS MGS catalogue comprises five bands photometry (u, g, r, i, z) and accurate redshift measurements from its spectroscopic observation. The central stellar velocity dispersion is measured within the 3'' diameter fiber. Derived quantities, like stellar mass and star formation rate (SFR), are obtained from multi-band photometric measurements and spectra indices (Kauffmann et al. 2003; Salim et al. 2016). In the present work, we adopt the stellar mass and SFR from the GALEX-SDSS-WISE Legacy Catalog (GSWLC) (Salim et al. 2016, 2018), which are estimated by fitting the UV-optical-IR bands photometry using the CIGALE code (Noll et al. 2009; Boquien et al. 2019) with the stellar library of Bruzual & Charlot (2003) and the initial mass function of Chabrier (2003). The specific star formation rate (SSFR) is defined as SFR/M_* . The middle panel of Fig. 1 shows the distribution of galaxies on the $M_* - \text{SFR}$ plane where one can clearly see the bimodality. We further separate galaxies into star-forming and quiescent populations, according to the method in Woo et al. (2013). We first fit a linear function to the star-forming main sequence by iteratively applying the least-square fitting and excluding data points 1 dex below the main sequence until convergence. Finally, we define galaxies with SFR lower than the main sequence by more than 1 dex as quiescent, and the remaining ones as star-forming. The separation line is

$$\log\left(\frac{\text{SFR}}{M_\odot/\text{yr}}\right) = 0.82 \times \log\left(\frac{M_*}{M_\odot}\right) - 9.17, \quad (1)$$

and shown as the black dashed line in the middle panel of Fig. 1.

Directly calculating the quiescent fraction in stellar mass bins for a magnitude-limited sample, like a r -band limited sample, will produce biased results, since star-forming galaxies are brighter in the blue band and hence they are preferentially selected, compared with their quiescent counterparts with similar stellar mass. In previous studies, a K -correction procedure is applied to all galaxies to calculate the V_{max} factors (Blanton & Roweis 2007), which are used for weighting these galaxies (e.g. Peng et al. 2010). A more conservative method is to construct a M_* -limited sample, which contains a complete sample of galaxies above some stellar mass threshold, which is a function of redshift (see Pozzetti et al. 2010, for more details), after which we can calculate a V_{max} factor for each

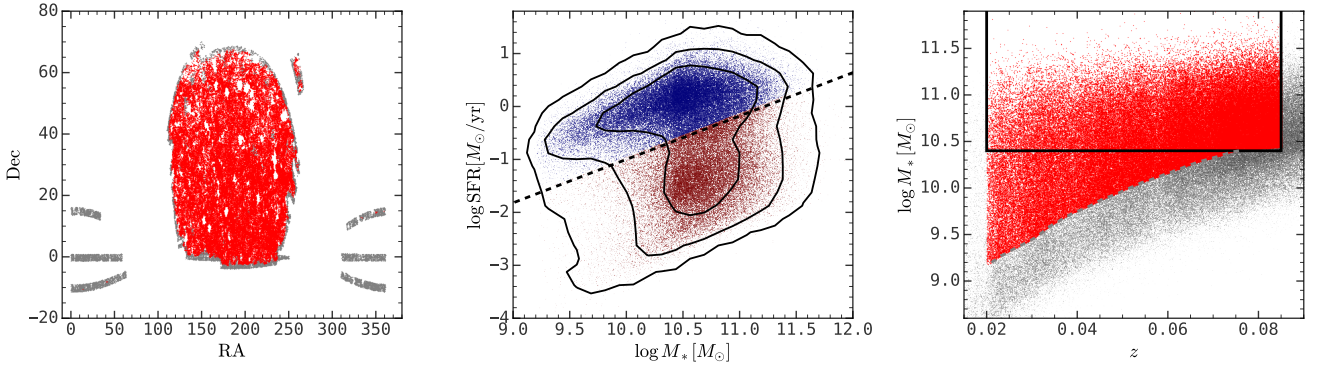


Figure 1. **Left panel:** The projected distribution of the SDSS main galaxy sample, where red points are the selected mass-limited galaxies with $f_{10\text{Mpc}} > 0.9$ and gray points are the remaining ones. **Middle panel:** The distribution of galaxies on the stellar mass and SFR plane with black solid lines enclose 68%, 95%, and 99.7% of the whole sample. The dashed line is the calibrated separation line for the star-forming and quiescent galaxies. The red points are quiescent galaxies and the blue ones are star-forming galaxies. **Right panel:** The distribution of galaxies on the redshift and stellar mass plane, where red points are the selected mass-limited galaxies with $f_{10\text{Mpc}} > 0.9$ and gray points are the remaining ones. The black solid lines enclose a volume-limited sample with $M_* > 10^{10.4} M_\odot$ and $0.02 < z < 0.09$. The central galaxies in the volume-limited sample, i.e. those enclosed by the black solid box, are environment definition tracers, while galaxies in the mass-limited sample, i.e. those above the black dashed line, are used for analysis, such as calculating the quiescent fraction.

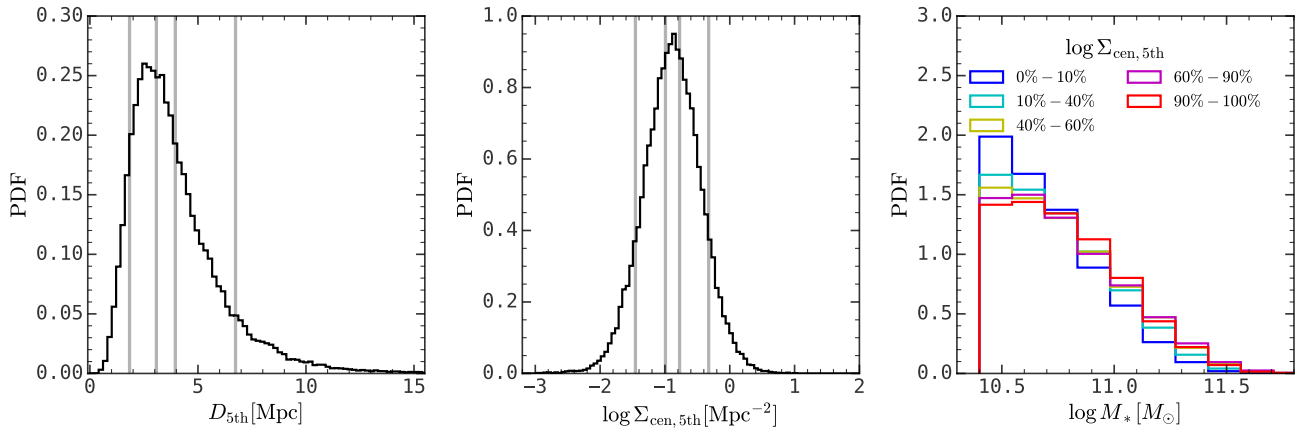


Figure 2. **Left panel:** The distribution of the projected distance to the 5th nearest central galaxy within $\pm 1000\text{km/s}$, i.e. $D_{5\text{th}}$, for the volume-limited sample, i.e. those in enclosed the black solid box on the left panel of Fig. 1. **Middle panel:** The distribution of the surface number density, i.e. $\Sigma_{\text{cen},5\text{th}}$, calculated with equation (4) for the volume-limited sample. **Right panel:** The distribution of stellar mass in different density quantiles for the volume-limited sample. The vertical lines in the first two panels correspond to the 10%, 40%, 60%, and 90% quantiles of $\Sigma_{\text{cen},5\text{th}}$ for all the mass-complete central galaxies. The vertical gray lines on the first two panels are the 10%, 40%, 60%, and 90% percentiles.

galaxy in the mass-limited sample. We adopted the latter in this paper. To begin with, we divide galaxies into small redshift bins, i.e. $\Delta z = 0.02$. Then, in each redshift bin, we select 20% galaxies with faintest r -band magnitude and calculate the rescaled stellar mass, i.e.

$$\log\left(\frac{M_{\text{scale}}}{M_\odot}\right) = \log\left(\frac{M_*}{M_\odot}\right) + 0.4 \times (r - r_{\text{lim}}) \quad (2)$$

where M_* and r are the stellar mass and r -band apparent magnitude, and r_{lim} is the limit r -band magnitude, which ranges from 17.57 to 17.72 for SDSS galaxies. Finally, the stellar mass limit is the envelope assembled by the 95% percentile of M_{scale} in each redshift bin. The envelope is shown as the gray dashed line on the right panel of Fig. 1 and the mass-limited sample is shown in red points. We also weigh each galaxy with $1/V_{\text{max}}$ where V_{max} is the volume

between z_{min} and z_{max} with $z_{\text{min}} = 0.02$ and z_{max} inferred from the mass-limited envelop calculated above according to the stellar mass of each galaxy (see also Wang et al. 2023a). In addition, we constructed a volume-limited sample by selecting galaxies with

$$M_* > 10^{10.4} M_\odot \quad \& \quad 0.02 < z < 0.09. \quad (3)$$

We emphasize that the central galaxies in the mass-limited sample are the objects for investigation in this work, and the central galaxies in the volume-limited sample only serve as environment tracers, which will be introduced in § 2.3.

We use the morphology classification from the Galaxy Zoo project¹ (Lintott et al. 2011). In Galaxy Zoo, galaxies are classified

¹ <https://data.galaxyzoo.org/>

as spiral, elliptical, and uncertain according to their image, and a debiasing process is applied. Here we define spiral galaxies as ones with the flag of SPIRAL set to one.

We use the group catalog of Yang et al. (2007) to select the central galaxy as the most massive one in each galaxy group. The halo mass is calibrated by abundance matching the total stellar mass with the theoretical halo mass function. We note that some studies require the central galaxy to be the most massive and the brightest one simultaneously. This more strict criterion only eliminates $\sim 2\%$ central galaxies from our sample (Peng et al. 2012), and has negligible impact on the results presented in this paper.

2.2 Simulation Data

The IllustrisTNG project (Pillepich et al. 2018a; Springel et al. 2018; Naiman et al. 2018; Marinacci et al. 2018; Pillepich et al. 2018b; Nelson et al. 2018, 2019) comprises a set of gravito-magnetohydrodynamical cosmological simulations that run with the moving mesh code AREPO (Springel 2010). It simulates the formation and evolution of galaxies from $z = 127$ to $z = 0$ based on a cosmology constrained in Planck Collaboration et al. (2016), where $\Omega_{\Lambda,0} = 0.6911$, $\Omega_{b,0} = 0.3089$, $\sigma_8 = 0.8159$, $n_s = 0.9667$, and $h = 0.6774$. In this paper, we are using the version with a box side length of $\sim 300\text{Mpc}$ for better statistics. This simulation contains 2500^3 dark matter particles with each weights $\sim 5.9 \times 10^7 M_{\odot}$, and $\sim 2500^3$ gas cells with each weights $\sim 1.1 \times 10^7 M_{\odot}$.

The dark matter halos are identified with the friends-of-friends (FoF) algorithm (Davis et al. 1985) using dark matter particles. Substructures are identified with the SUBFIND algorithm using all types of particles (Springel et al. 2001), then the baryonic components are defined as galaxies and the dark matter components are defined as subhalos. In each FoF halo, the central subhalo is defined as the one that is located at the minimum of the gravitational potential, and the galaxy inside this subhalo is defined as the central galaxy, while the remaining subhalos and galaxies are satellites. Subhalo merger trees are constructed using the SUBLINK algorithm (Rodríguez-Gomez et al. 2015), and we identify the main progenitor for each subhalo/galaxy as the one with the most massive progenitor history (De Lucia & Blaizot 2007).

Here we define the halo mass for each FoF halo as the total mass within a radius within which the average density equals 200 times the critical density, while the radius is used as the halo radius and denoted as R_{200} . The stellar mass is calculated by summing all the stellar particle mass within $2R_*$, where R_* is the stellar half-mass radius for all the stellar particles attributed to the subhalo. The SFR is also calculated from all the star-forming particles within $2R_*$. For galaxies in the IllustrisTNG simulation, those with $\text{SSFR} < 10^{-11} \text{yr}^{-1}$ are defined as quiescent, while the remaining ones are star-forming. It is noteworthy that we are using a different criterion to separate star-forming/quiescent galaxies in observation and simulation. Since we do not intend to perform a quantitative comparison between simulation and observation (e.g. Donnari et al. 2019, 2021), it is fine as long as this separation criterion does not bias the environmental dependence of the quiescent fraction.

For all central galaxies at $z = 0$, we also identify a sub-sample of backplash galaxies with the following properties (Wang et al. 2009; Wetzel et al. 2014):

- (i) They are central galaxies at $z = 0$.
- (ii) Their main progenitors were once satellites of other halos and the satellite state lasts at least two successive snapshots. Here

the second requirement is to avoid the *central-satellite switching problem* (see Figure 1 in Poole et al. 2017).

2.3 Large-scale environment

The formation and evolution of galaxies and their associated dark matter halos are subject to environmental effects (Mo et al. 2010). There are many different metrics to quantify galaxy environments on different spatial scales (e.g. Muldrew et al. 2012). Here we define a novel environment metric that only uses central galaxies as tracers, which is defined as

$$\Sigma_{\text{cen},5\text{th}} = \frac{5}{\pi D_{5\text{th}}^2} \quad (4)$$

where $D_{5\text{th}}$ is the projected distance to the fifth nearest central galaxy within $\pm 1000\text{km/s}$ in the volume-limited galaxy sample. And each central galaxy in the mass-limited sample has a value of $\Sigma_{\text{cen},5\text{th}}$ calculated. The choice of the fifth neighbor is motivated by two reasons. On one side, it cannot be too small which will suffer from the shot noise. On the other side, it cannot be too large where all the information will be smoothed out. Finally, we choose to use the fifth nearest neighbor.

The search of the nearest neighbors can be seriously biased near the edge of survey regions and bright star masks. For the validity of our environment metric, we exclude central galaxies whose 5th nearest neighbor searching is biased. We randomly drop one million points in a rectangular region that enclose the survey footprint on the sphere. Then, we calculate a completeness factor for each central galaxy, which is defined as

$$f_R = \frac{N(< \theta)}{\pi \theta^2 \bar{\Sigma}}, \quad \theta = R/D_A \quad (5)$$

where $N(< \theta)$ is the number of random points within the survey mask and within an angular distance of θ from the central galaxy in question (Blanton et al. 2005), and $\bar{\Sigma}$ is the mean surface density of random points, and D_A is the angular distance of the central galaxy in question. In the present work, we restrict our study to central galaxies with $f_{10\text{Mpc}} > 0.9$, where 10Mpc is larger than the $D_{5\text{th}}$ for most of the central galaxies in this study, and we present the projected distribution of these selected galaxies with red points on the left panel of Fig. 1. We note that the spatial incompleteness can bias the environment estimation by underestimating the local density for galaxies near masked regions, so we make a conservative cut of 90% completeness to mitigate this effect. It is also noteworthy that this effect can only undermine the environmental dependence of galaxy properties rather than inducing it as long as the spatial mask does not correlate with the galaxy properties in question.

In Fig. 2, we present the distribution of $D_{5\text{th}}$ and $\Sigma_{\text{cen},5\text{th}}$ for all central galaxies in the volume-limited sample on the first two panels, with vertical lines indicate the 10%, 40%, 60%, and 90% percentiles. One can see that $D_{5\text{th}}$ spans a large range from $\lesssim 1\text{Mpc}$ to $\gtrsim 10\text{Mpc}$. The middle panel shows the distribution of $\Sigma_{\text{cen},5\text{th}}$. On the right panel, we plot the stellar mass distributions for central galaxies in the M_* -limited sample with different central-traced densities. One can clearly see that the high-density regions are preferentially occupied by massive galaxies.

3 RESULTS

Fig. 3 shows the median SSFR and the quiescent fraction of central galaxies on the $M_* - \Sigma_{\text{cen},5\text{th}}$ plane. The most obvious feature is

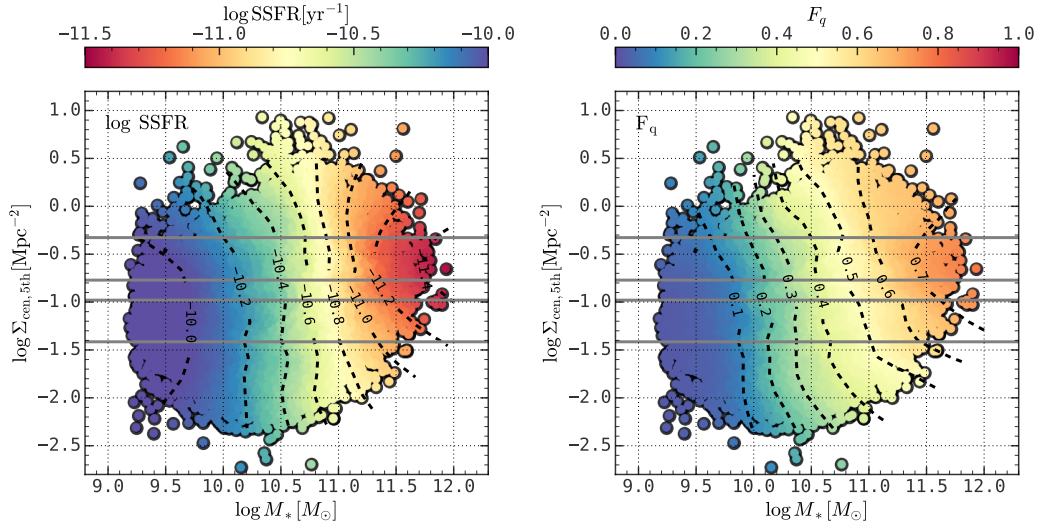


Figure 3. The median SSFR (**left panel**) and quiescent fraction (**right panel**) on the $\Sigma_{\text{cen},5\text{th}}$ - stellar mass plane for SDSS galaxies, smoothed with the LOESS method. The black dashed lines are the contour lines and the horizontal gray solid lines are the 10%, 40%, 60%, and 90% percentiles of $\Sigma_{\text{cen},5\text{th}}$. For better visual illustration, we restrict the SSFR of galaxies to be within $(10^{-11.5}, 10^{-10})\text{yr}^{-1}$ on the right panel.

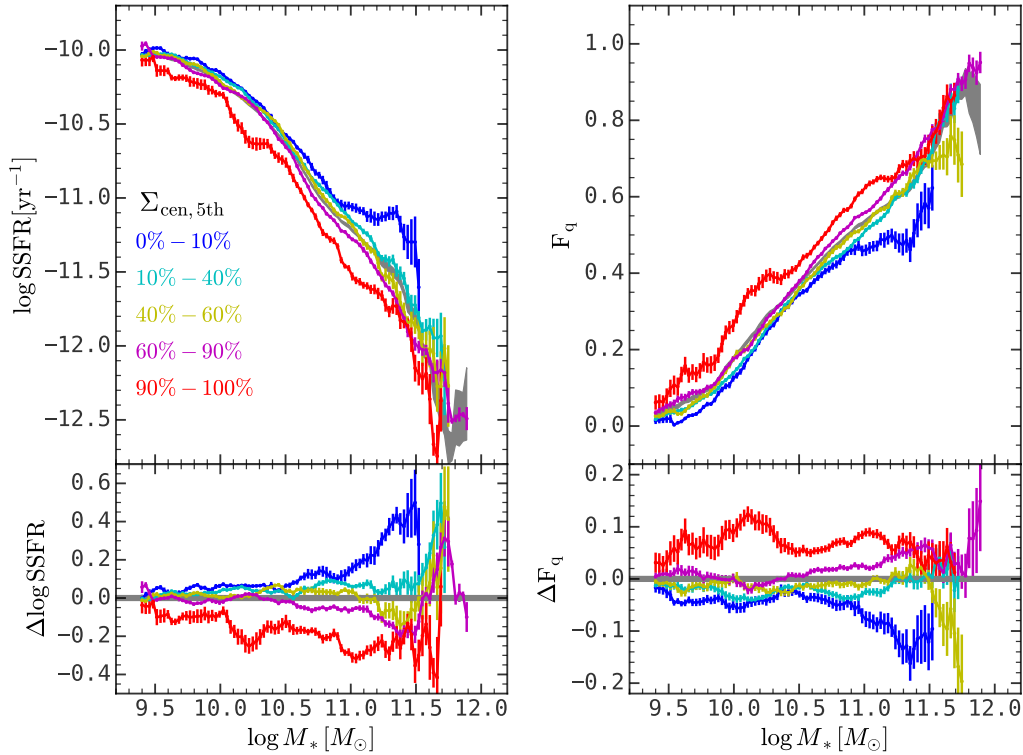


Figure 4. Top panels: The median SSFR (**left panel**) and the quiescent fraction (**right panel**) as a function of stellar mass in different $\Sigma_{\text{cen},5\text{th}}$ bins for SDSS galaxies. The gray regions are for all of the central galaxies. Error bars are calculated from bootstrap samples. **Bottom panels:** The residual with respect to the result for all of the central galaxies, i.e. the gray regions on top panels.

that the gradient aligns with stellar mass, consistent with previous works (Peng et al. 2012). For low-mass central galaxies ($M_* \lesssim 10^{10.5} M_\odot$), one can see a weak dependence on $\Sigma_{\text{cen},5\text{th}}$ from the inclined contour lines, especially above the 90% quantile. This weak trend indicates that low-mass central galaxies have lower SSFR and are more quenched in these dense regions. Finally, the contour lines are also weakly inclined for massive galaxies ($M_* \gtrsim 10^{11} M_\odot$) with low $\Sigma_{\text{cen},5\text{th}}$, indicating that these galaxies are more star-forming and less quenched than those with high $\Sigma_{\text{cen},5\text{th}}$. We note that these two trends are the manifestations of the two-halo galactic conformity effect for central galaxies.

To see these signals more clearly, Fig. 4 shows the median SSFR and the quiescent fraction as a function of stellar mass in five $\Sigma_{\text{cen},5\text{th}}$ bins. From the right panel of Fig. 2, one can see that dense regions prefer to host massive galaxies, which is consistent with previous results that massive galaxies are more clustered than low-mass ones (Mo & White 1996; Li et al. 2006, 2013; Wang et al. 2016). Consequently, galaxies in higher-density regions are on average more massive than those in relatively low-density regions in the same finite stellar mass bin, and this will induce an artificial dependence on $\Sigma_{\text{cen},5\text{th}}$. Thus, following the method of Hartley et al. (2015), we construct histograms with narrow stellar mass bins, i.e. $\Delta \log M_* = 0.1$, and calculate a weighting factor for each central galaxy, which is

$$w_i^j = N_i / N_i^j \quad (6)$$

where w_i^j is the weight for a central galaxy in the i -th M_* bin and the j -th $\Sigma_{\text{cen},5\text{th}}$ bin, N_i is the number of central galaxies in the i -th M_* bin, and N_i^j is the number of central galaxies in the i -th M_* bin and j -th $\Sigma_{\text{cen},5\text{th}}$ bin simultaneously (see also Kawinwanichakij et al. 2016).

In Fig. 4, the gray shaded regions show the results for central galaxies regardless of their $\Sigma_{\text{cen},5\text{th}}$, and solid lines with different colors show the results for central galaxies in five $\Sigma_{\text{cen},5\text{th}}$ bins with error bar calculated using the bootstrap method. Meanwhile, the lower panels show the deviation from the results for all central galaxies. As one can see, central galaxies in the densest regions are ~ 10 percent more quenched than those in the lowest $\Sigma_{\text{cen},5\text{th}}$ -bin, and the SSFR is also lower by ~ 0.2 dex. Moreover, we also find that the galaxies with $M_* > 10^{11} M_\odot$ in the lowest-density regions are less quenched than their counterparts in more dense regions by ~ 15 percent, and the median SSFR is also lower by ~ 0.4 dex. Although the star formation of central galaxies only weakly depends on $\Sigma_{\text{cen},5\text{th}}$, this dependence is statistically significant, which can be seen from the small error bars estimated with the bootstrap method.

4 DISCUSSION

4.1 Conformity signal for low-mass central galaxies

Fig. 4 shows that low-mass galaxies with $M_* \lesssim 10^{10.5} M_\odot$ residing in high-density regions are more quenched than their counterparts in low-density regions. This phenomenon is not only found in observation, but also shown in the semi-analytical models (SAMs) and hydrodynamical simulations of galaxy formation (e.g. Lacerna et al. 2018, 2022; Ayromlou et al. 2022). Lacerna et al. (2022) uses the IllustrisTNG simulation and the SAM of SAG (e.g. Springel et al. 2001; Cora et al. 2018) to demonstrate that this effect is attributed to the vicinity of low-mass central galaxies around massive clusters, so it disappears once these galaxies are removed. Similarly, Ayromlou et al. (2022) find that the original SAM of L-GALAXIES in

Henriques et al. (2015) has no conformity signal until a new recipe is adopted, where the ram-pressure stripping effect can also affect the evolution of galaxies beyond the virial radius of massive halos (Ayromlou et al. 2021).

Here we use the IllustrisTNG simulation to see the dependence of central-galaxy properties on large-scale environments and explore their physical origins. Since we intend to study similar signals in IllustrisTNG instead of performing a quantitative comparison with observation, there is no need to include observation effects like the redshift-space distortion effect, which can only undermine the strength of this conformity signal. Here we define a 3D-version large-scale environment metric of equation 4 for each central galaxy, i.e.

$$\rho_{\text{cen},5\text{th}} = \frac{3 \times 5}{4\pi D_{5\text{th}}^3} \quad (7)$$

where $D_{5\text{th}}$ is the distance to the 5th nearest central galaxy.

Fig. 5 shows the quiescent fraction of central galaxies as a function of stellar mass in different bins of $\rho_{\text{cen},5\text{th}}$, where the left panel shows the result for all central galaxies. Clearly, one can see that low-mass central galaxies with $M_* \lesssim 10^{10.5} M_\odot$ in dense regions are more quenched than their counterparts in under-dense regions and the difference in the quiescent fraction is up to 12%. The middle panel of Fig. 5 shows the result after removing all backsplash central galaxies, which are central galaxies at $z = 0$ and were satellite galaxies in other halos at $z < 1^2$. Here one can see that the conformity signal completely disappears on the whole stellar mass range. This result suggests that the conformity signal for low-mass central galaxies in the IllustrisTNG simulation mainly comes from the backsplash galaxies (Wetzel et al. 2014). As suggested in Wetzel et al. (2014), we can also eliminate the impact of backsplash galaxies by removing galaxies within $4R_{200}$ of any other more massive halos, and the result is shown on the right panel of Fig. 5. Here we can see that the conformity signal for galaxies with $M_* \lesssim 10^{10.5} M_\odot$ also disappears.

Previous studies quantify the two-halo galactic conformity effect with the quiescent fraction difference of neighboring galaxies (*secondary galaxies*) around star-forming and quiescent central galaxies (*primary galaxies*). Lacerna et al. (2022) found that galaxies around quiescent central galaxies are more quenched than those around star-forming central galaxies with similar stellar masses in the IllustrisTNG simulation, and this difference is prominent up to ~ 10 Mpc (see also Ayromlou et al. 2022). Here we want to see if backsplash galaxies can explain the two-halo galactic conformity signal manifested in this way. In previous studies, the primary galaxies only include centrals, and the secondary galaxies include both centrals and satellites. As we argued in § 1 (see also § 4.3), the mixing of central and satellite galaxies makes the result hard to interpret, so here we only include centrals for both the primary and the secondary galaxies.

Fig. 6 shows the quiescent fraction of central galaxies with $M_* \geq 10^9 M_\odot$ (secondary galaxies) as a function of distance to central galaxies in three stellar mass bins (primary galaxies). The primary galaxies are further separated into star-forming and quiescent populations and the results are shown in blue and red colors, respectively. Top panels in Fig. 6 show the results for all central galaxies in the TNG simulation. Here one can see that secondary galaxies

² Here we only consider backsplash galaxies that were satellite galaxies at $z < 1$ since, at higher redshift, the progenitor galaxies have very low stellar mass and suffer from resolution problems.

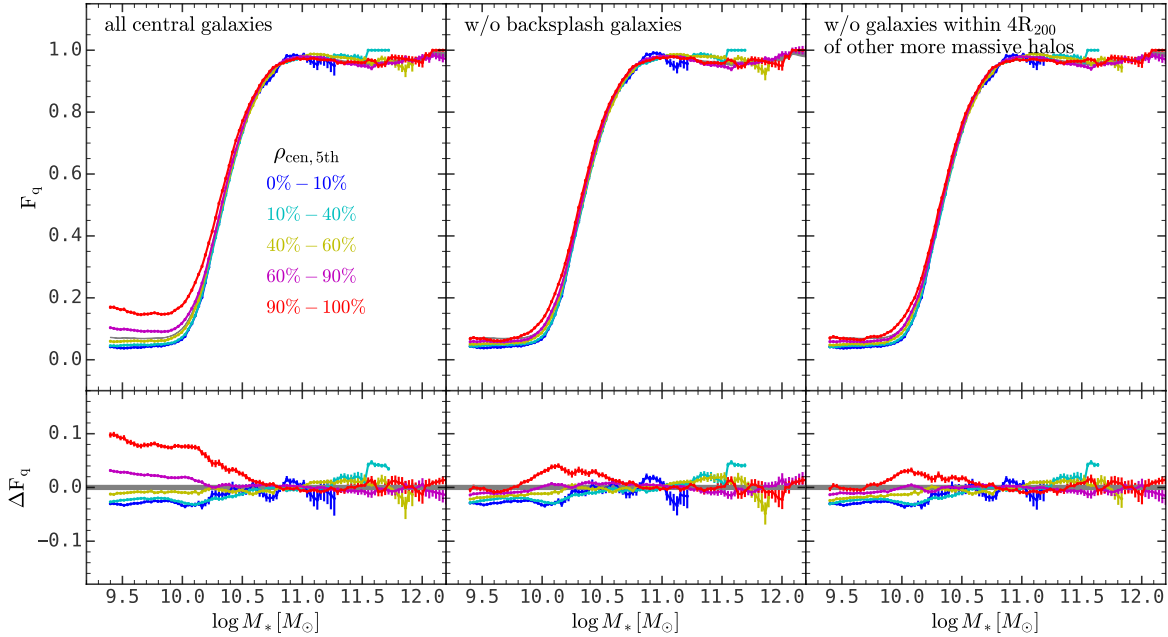


Figure 5. Upper panels: The quiescent fraction as a function of stellar mass in different $\rho_{\text{cen},5\text{th}}$ quantiles in the IllustrisTNG simulation at $z = 0$. The gray filler regions are the results for all central galaxies. Error bars are calculated from bootstrap samples. **Lower panels:** The residual of the quiescent fraction with respect to the result for all central galaxies. The first column shows the result for all central galaxies. The second column shows the result after removing all backsplash galaxies (see § 2.2). The last column shows the result after removing all central galaxies within $4R_{200}$ of any other more massive halos. One can see that the environmental dependence of the quiescent fraction for low-mass central galaxies in the IllustrisTNG simulation can be entirely explained by backsplash galaxies. And the IllustrisTNG simulation cannot reproduce the signal for massive galaxies as we have seen in observation (see Fig. 4).

around quiescent primary galaxies have higher quiescent fraction by $\lesssim 20\%$, and the difference in the quiescent fraction decreases for more massive primary galaxies and for larger separations, until the difference disappears for the primary galaxies with $M_* \gtrsim 10^{10} M_\odot$ or for $r > 8$ Mpc. Panels on the second row in Fig. 6 show the result after removing all backsplash central galaxies. Here one can see that the difference in the quiescent fraction for star-forming and quiescent primary galaxies disappears, indicating that the two-halo galactic conformity signal comes from these backsplash galaxies. Finally, we tested the method suggested in Wetzel et al. (2014) to eliminate the impact of backsplash galaxies by removing centrals within $4R_{200}$ of any other more massive halos, and the result is shown on the bottom panels in Fig. 6. Again, the conformity signal completely disappears. It is noteworthy that previous studies have shown that low-mass central galaxies close to more massive halos are more likely to be backsplash galaxies (Wetzel et al. 2014), which is also consistent with the result here.

In order to further understand the distribution of backsplash galaxies around massive halos and their contribution to the two-halo conformity signal for central galaxies, we select all central galaxies around halos with $M_h \geq 10^{13} M_\odot$ in the IllustrisTNG simulation and calculate their quiescent fractions and backsplash fractions in Fig. 7. The quiescent fractions of central galaxies around these massive halos are shown in gray circles as a function of normalized distance. Here one can see prominent quiescent fraction excess for central galaxies in the vicinity of these massive halos, which is a manifestation of the two-halo conformity effect for central galaxies. Then, we separate these central galaxies into the backsplash ones and non-backsplash ones and plot their quiescent fractions in red and blue colors, respectively. Here one can see that the quiescent fraction

for non-backsplash central galaxies shows no excess anymore and coincides with the average quiescent fraction for all non-backsplash galaxies in the simulation volume. This indicates that the quiescent fraction excess around massive halos in the IllustrisTNG simulation, which is responsible for the two-halo conformity effect for central galaxies, all stems from backsplash galaxies. Meanwhile, the right y-axis of Fig. 7 shows the fraction of backsplash galaxies among all central galaxies around these massive halos, where the backsplash galaxies range from 20% to 80%. We note that backsplash galaxies dominate ($>50\%$) the central galaxy population within $2R_{200}$ around these massive systems and gradually declines to $\lesssim 20\%$ around $4R_{200}$. Eventually, they will approach the average fraction (5%–10%) in the simulation volume, as shown in magenta horizontal dotted lines. We note that those distant backsplash galaxies are not all associated with the halos in question and, instead, from other nearby massive halos (Wetzel et al. 2014). This figure clearly demonstrates that the mere presence of massive halos around central galaxies cannot affect their star formation states, and more violent within-halo environmental processes are required. Nevertheless, it is noteworthy that non-backsplash central galaxies in the vicinity of massive halos may suffer from some other environmental effects, like the termination of gas accretion and the stripping of the circumgalactic medium, as found in previous studies (e.g. Bahé et al. 2013; Behroozi et al. 2014; Ayromlou et al. 2021).

The above results clearly demonstrate that the conformity signal in the IllustrisTNG simulation can be entirely explained by backsplash galaxies. In real observation, since we have no access to their halo merger trees, we can only eliminate the impact of backsplash galaxies by removing galaxies close to any other more massive halos. Here we remove all central galaxies within $4R_{200}$

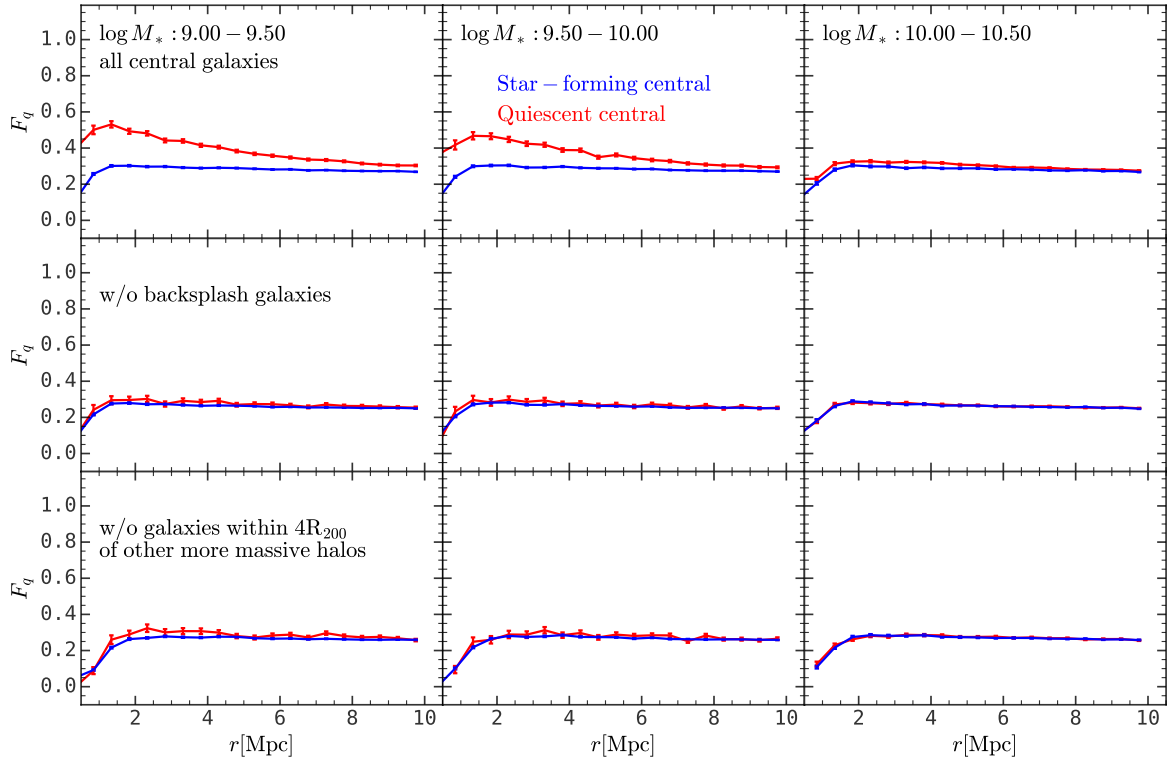


Figure 6. The quiescent fraction for central galaxies with $M_* \geq 10^9 M_\odot$ as a function of distance to central galaxies in three stellar mass bins in the IllustrisTNG simulation. Panels on the first row are for all central galaxies. The panels on the second row are for all central galaxies except backsplash ones. Panels on the third are for all central galaxies except those within $4R_{200}$ of any other more massive halos. These results also indicate that the two-halo conformity effect for central galaxies in the IllustrisTNG simulation can be entirely explained by backsplash galaxies.

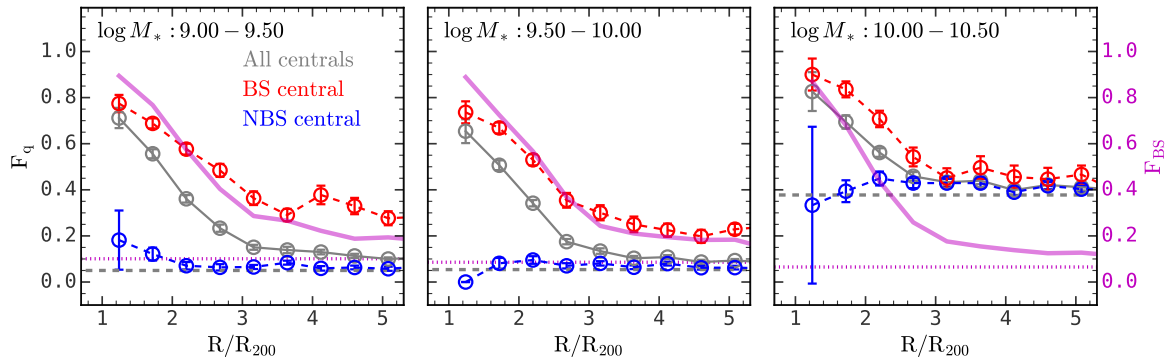


Figure 7. **Left y-axis:** The quiescent fraction of central galaxies around dark matter halos with $M_h \geq 10^{13} M_\odot$ as a function of normalized distance in three stellar mass bins in the IllustrisTNG simulation. The gray circles show the results for all central galaxies, the red circles are for all backsplash galaxies, and the blue circles are for all non-backsplash galaxies. Error bars are estimated as the standard deviation of bootstrap samples. The gray horizontal dashed lines are the average quiescent fraction for all non-backsplash central galaxies in the simulation volume in three stellar mass bins. **Right y-axis:** The magenta lines show the fraction of the backsplash galaxies among all central galaxies around halos with $M_h \geq 10^{13} M_\odot$ in the IllustrisTNG simulation. The magenta horizontal dotted lines are the average fraction of backsplash galaxies among all central galaxies in the simulation volume in three stellar mass bins. This figure demonstrates that the quiescent fraction excess for central galaxies around massive halos in the IllustrisTNG simulation all stems from backsplash galaxies.

of any other more massive halos with $\Delta V < 1000 \text{ km/s}$, and Fig. 8 shows the resulting median SSFR and the quiescent fraction for central galaxies as a function of stellar mass and $\Sigma_{\text{cen},5\text{th}}$. Here one can see that the dependence of SSFR and quiescent fraction on $\Sigma_{\text{cen},5\text{th}}$ are nearly eliminated, indicating this conformity signal is mainly

due to the presence of backsplash galaxies. Again, we can still see a weak dependence on $\Sigma_{\text{cen},5\text{th}}$. This is consistent with the weak signal presented in Tinker et al. (2017), in which they suggest that this signal is attributed to the correlation between halo formation histories and the star formation activities of central galaxies.

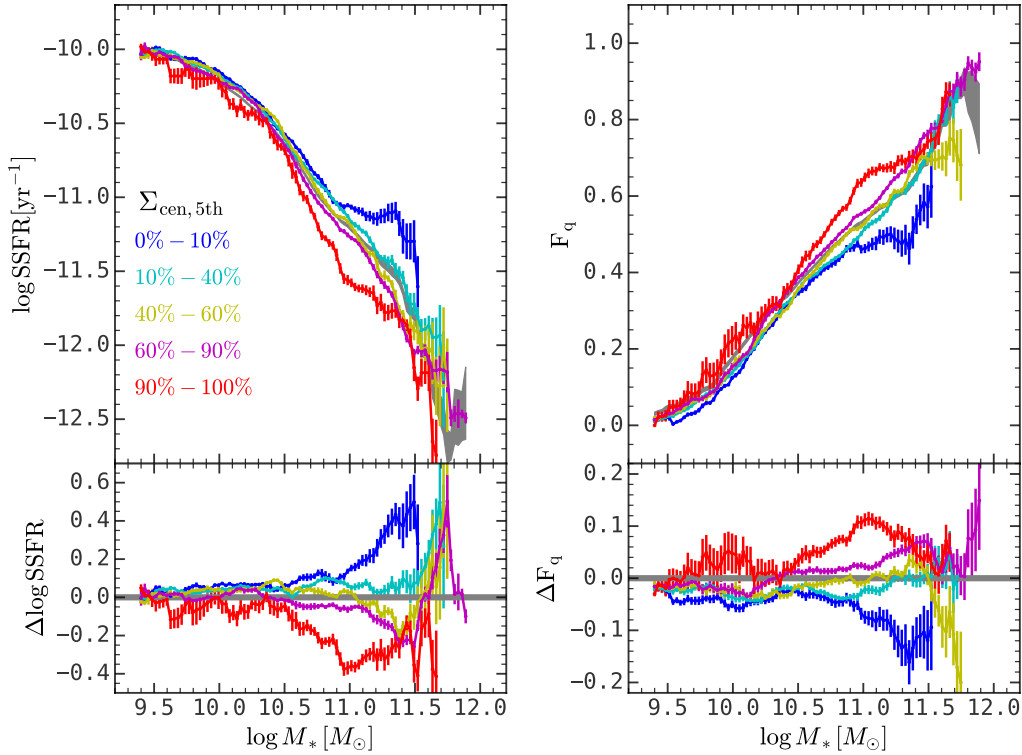


Figure 8. Similar to Fig. 4. Here we exclude galaxies within $4R_{200}$ of any other more massive halos with $\Delta V < 1000 \text{ km/s}$. One can see that the conformity signal for low-mass galaxies are largely eliminated, indicating that this effect is mainly contributed by backplash galaxies.

Finally, we want to emphasize that the results in Fig. 5 and Fig. 6 only indicate that the two-halo conformity effect for central galaxies in IllustrisTNG can be explained by backplash galaxies, but cannot falsify the existence of super-halo-scale environmental effects on low-mass central galaxies. Our results highlight the role played by these backplash galaxies, even though only 20% – 80% of the central galaxies around massive halos are backplash galaxies (see Fig. 7). We also emphasize the necessity to control the contribution from these galaxies before we can study the impact of super-halo-scale environmental effects. Finally, investigations on other models can help us better understand the environmental effect, within-halo and super-halo-scale, on galaxies. For example, Ayromlou et al. (2022) performs a similar analysis on the semi-analytical of Ayromlou et al. (2021), where they found that the two-halo conformity effect on central galaxies is still prominent after removing backplash galaxies from the primary sample and all satellite galaxies are retained in the secondary sample (see their Figure 8).

4.2 Conformity signal for massive central galaxies

From Fig. 4, we can also see that massive central galaxies with $M_* \gtrsim 10^{11} M_\odot$ show strong dependence on $\Sigma_{\text{cen},5\text{th}}$, where those in low-density regions are more star-forming than their counterparts in dense regions. Moreover, this dependence is still there after the elimination of the backplash galaxies (See Fig. 8), indicating that this effect cannot be attributed to these backplash galaxies. A related trend was also pointed out in Tinker et al. (2018a), where they focused on star-forming galaxies and found that star-forming central galaxies preferentially live in low-density regions.

Recently, Zhang et al. (2022) found that star-forming massive

central galaxies prefer to reside in low-mass halos than their quiescent counterparts based on weak lensing measurements (see also Mandelbaum et al. 2006; More et al. 2011; Rodriguez-Gomez et al. 2015; Mandelbaum et al. 2016; Zhang et al. 2021a). Consequently, these star-forming central galaxies are less clustered than those quiescent ones (see also Figure 6 of their paper), as expected since massive halos have higher clustering strength (Mo & White 1996). This result qualitatively agrees with findings in this paper.

To understand the origin of this signal, we investigated their morphology and kinematics, and the results are presented in Fig. 9. On the left panel, we can see that these massive galaxies ($M_* \gtrsim 10^{11} M_\odot$) in low-density regions are preferentially spiral compared with massive galaxies in dense regions. Meanwhile, from the right panel, one can see that the median central stellar velocity dispersion is also lower for massive galaxies in sparse regions than their counterparts in dense regions by $\sim 15\%$, indicating relatively low-mass bulges and central black holes. All these results together suggest a simple explanation for the conformity signal we observed here. Galaxies in sparse regions experienced fewer merger events (Fakhouri & Ma 2009; Jian et al. 2012; Kampeczyk et al. 2013), thus their spiral morphology keeps intact and the growths of their bulge and central black hole are suppressed. Consequently, they are less likely to be quenched. This explanation is also supported by Posti et al. (2019), where they found that spiral galaxies can convert baryons to stars much more efficiently than galaxies with non-spiral morphology (see also Posti & Fall 2021; Mancera Piña et al. 2022).

It is noteworthy that the IllustrisTNG simulation cannot reproduce the conformity signal for massive galaxies. In the IllustrisTNG model, the star formation activities of massive central galaxies are mostly determined by the integrated kinetic energy released by the

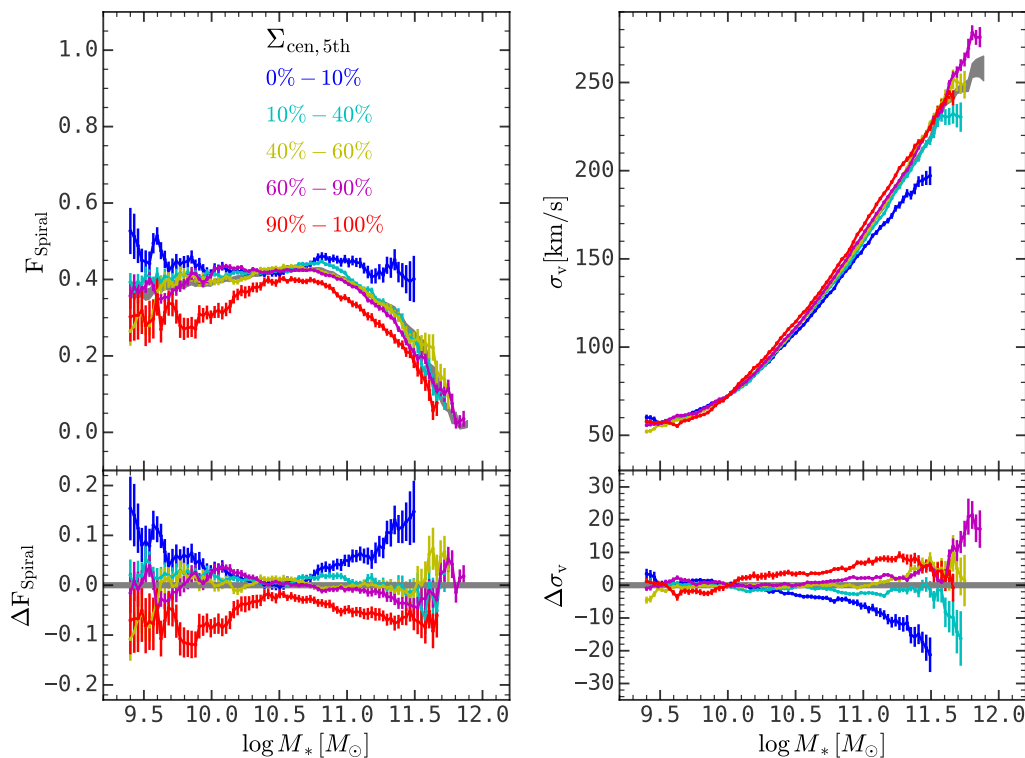


Figure 9. The fraction of spiral galaxies (**left panel**) and the median central stellar velocity dispersion (**right panel**) for central galaxies as a function of stellar mass in different $\Sigma_{\text{cen}, 5\text{th}}$ bins for SDSS galaxies. Error bars are calculated from bootstrap samples. And the lower panels show the residual with respect to the results for all of the central galaxies at given stellar mass.

AGN feedback process, or equivalently, the black hole mass (Terrazas et al. 2020; Xu & Peng 2021; Piotrowska et al. 2022; Bluck et al. 2022). Meanwhile, the mass of central massive black holes strongly correlates with the total stellar mass of their host galaxies (Terrazas et al. 2020; Habouzit et al. 2021). Consequently, the star formation activities of massive central galaxies ($\geq 10^{11} M_{\odot}$) are mostly quenched due to the possession of massive black holes and have no dependence on their large-scale structure. In observation, the star formation activities of central galaxies also mostly depend on the mass of their central black hole (Piotrowska et al. 2022). However, observational results reveal a tight relation between black hole masses and bulge masses (e.g. Magorrian et al. 1998; Kormendy et al. 2011; Kormendy & Ho 2013), and the relation between bulge masses and the stellar masses of host galaxies is not tight due to a broad distribution of the bulge-to-total mass ratio (B/T) (e.g. Davis et al. 2018), where massive star-forming central galaxies tend to have lower B/T than their quiescent counterparts (Zhang et al. 2021b; Shi et al. 2022).

4.3 Two-halo conformity effect on satellite galaxies

In this work, we only consider central galaxies in the secondary galaxy sample, while previous studies on the two-halo conformity effect include both central and satellite galaxies. We emphasize that it is helpful to separate these two populations of galaxies for a better understanding of the underlying physical drivers of the two-halo conformity effect.

Before one can study the impact of the two-halo conformity

effect on satellite galaxies³, it is necessary to carefully control the within-halo environmental effect from their own host halos. Previous studies, from both observations and simulations, reveal that the within-halo environmental effect severely affects the properties of satellite galaxies by shutting down the new gas replenishment, stripping the existing cold gas content, and quenching their star formation activities. And the major determinants for the within-halo environmental effect are halo mass and halo-centric distance (e.g. Woo et al. 2013; Wang et al. 2018). Consequently, in order to study the impact of the two-halo conformity on satellite galaxies, one must control the influence of their own host halos, which is beyond the scope of this paper.

Moreover, previous studies found that quiescent central galaxies prefer to live in more massive halos than their star-forming counterparts (e.g. Mandelbaum et al. 2016; Zhang et al. 2022), which is related to the one-halo conformity effect where halos with quiescent central galaxies prefer to host quiescent satellites (Weinmann et al. 2006). Combined with the fact that more massive halos are more clustered (e.g. Mo & White 1996), satellite galaxies can exhibit the two-halo conformity signal without any new physical processes introduced.

³ Satellite galaxies can be within or beyond halo virial radius due to the anisotropic spatial distribution of halos.

5 CONCLUSION

Previous studies show that the star formation activities of central galaxies are primarily determined by their stellar mass. In addition, their star formation activities are also found to be in correlation over several Mpc. This is known as the two-halo galactic conformity effect, and its physical origin is still under debate. In this paper, we studied one manifestation of the two-halo galactic conformity effect by investigating the dependence of the star formation activities of central galaxies on the large-scale environment. Our main results are summarized as follows:

(i) We proposed a novel large-scale environment metric, $\Sigma_{\text{cen},5\text{th}}$, which is inferred from the distance to the fifth nearest central galaxy. This metric measures the environment from ~ 1 Mpc to ≥ 10 Mpc, with a median value of ~ 4 Mpc. With this environment metric, we found two kinds of minor but significant dependence on $\Sigma_{\text{cen},5\text{th}}$. The first one is that central galaxies in the highest-density regions are more quenched by ~ 10 percent than those in the lowest-density regions, and the median SSFR is lower by ~ 0.2 dex. The second one is that massive central galaxies in the lowest-density regions are less quenched by ≥ 15 percent than those in the highest-density regions, and the median SSFR is also higher by ~ 0.4 dex (see Fig. 4).

(ii) We found a similar trend in the IllustrisTNG simulation where low-mass central galaxies are more quenched in dense regions than those in sparse regions by $\lesssim 12$ percent. We found that this signal is mainly contributed by backplash galaxies, which are central galaxies that once were satellites of other halos, so the environmental dependence of the quiescent fraction for low-mass central galaxies disappears once these backplash galaxies are removed. The impact of these backplash galaxies can also be eliminated by removing central galaxies in the vicinity of more massive halos in the IllustrisTNG simulation. By applying the same procedure to the observational data, we found that the environmental dependence of the quiescent fraction for low-mass central galaxies is largely reduced, suggesting the conformity signal for low-mass central galaxies in observation also comes from backplash galaxies (see Fig. 5 and Fig. 8).

(iii) We found that the two-halo galactic conformity effect for central galaxies manifested by the quiescent fraction difference of neighboring central galaxies (secondary galaxies) around star-forming and quiescent central galaxies (primary galaxies) decreases with increasing the stellar mass of primary galaxies and increasing the separation between the primary and the secondary galaxies in the IllustrisTNG simulation, which is consistent with previous results. Most importantly, we found that this signal can be entirely explained by backplash galaxies, where this signal completely disappears once backplash galaxies are removed (see Fig. 6).

(iv) Massive central galaxies in the lowest-density regions are not only more star-forming, but also have a higher fraction of spiral morphology by ~ 15 percent and lower median central stellar velocity dispersion by ~ 10 percent. These results suggest a simple scenario that these galaxies in sparse regions on average have experienced fewer major merger events, and as a consequence, they have higher disk frequency, lower central stellar velocity dispersion, less massive central black holes. Hence they are more likely to survive from star formation suppression processes, including merging-quenching, morphological quenching and AGN feedback that are closely related to a massive classical bulge and a massive black hole (see Fig. 9).

ACKNOWLEDGEMENTS

The authors thank the anonymous referee for their helpful comments that improved the quality of the manuscript. This work is supported by the National Science Foundation of China (NSFC) Grant No. 12125301, 12192220, 12192222, and the science research grants from the China Manned Space Project with NO. CMS-CSST-2021-A07.

The authors acknowledge the Tsinghua Astrophysics High-Performance Computing platform at Tsinghua University for providing computational and data storage resources that have contributed to the research results reported within this paper.

Funding for the SDSS and SDSS-II has been provided by the Alfred P. Sloan Foundation, the Participating Institutions, the National Science Foundation, the U.S. Department of Energy, the National Aeronautics and Space Administration, the Japanese Monbukagakusho, the Max Planck Society, and the Higher Education Funding Council for England. The SDSS Web Site is <http://www.sdss.org/>.

The SDSS is managed by the Astrophysical Research Consortium for the Participating Institutions. The Participating Institutions are the American Museum of Natural History, Astrophysical Institute Potsdam, University of Basel, University of Cambridge, Case Western Reserve University, University of Chicago, Drexel University, Fermilab, the Institute for Advanced Study, the Japan Participation Group, Johns Hopkins University, the Joint Institute for Nuclear Astrophysics, the Kavli Institute for Particle Astrophysics and Cosmology, the Korean Scientist Group, the Chinese Academy of Sciences (LAMOST), Los Alamos National Laboratory, the Max-Planck-Institute for Astronomy (MPIA), the Max-Planck-Institute for Astrophysics (MPA), New Mexico State University, Ohio State University, University of Pittsburgh, University of Portsmouth, Princeton University, the United States Naval Observatory, and the University of Washington.

DATA AVAILABILITY

The data underlying this article will be shared on reasonable request to the corresponding author. The computation in this work is supported by the HPC toolkit **HIPP** at <https://github.com/ChenYangyao/hipp>.

REFERENCES

- Abazajian K. N., et al., 2009, *The Astrophysical Journal Supplement Series*, 182, 543
- Ayromlou M., Kauffmann G., Yates R. M., Nelson D., White S. D. M., 2021, *Monthly Notices of the Royal Astronomical Society*, 505, 492
- Ayromlou M., Kauffmann G., Anand A., White S. D. M., 2022, *Monthly Notices of the Royal Astronomical Society*
- Bahé Y. M., McCarthy I. G., Balogh M. L., Font A. S., 2013, *Monthly Notices of the Royal Astronomical Society*, 430, 3017
- Baldry I. K., Balogh M. L., Bower R. G., Glazebrook K., Nichol R. C., Bamford S. P., Budavari T., 2006, *Monthly Notices of the Royal Astronomical Society*, 373, 469
- Ball N. M., Loveday J., Brunner R. J., Baldry I. K., Brinkmann J., 2006, *Monthly Notices of the Royal Astronomical Society*, 373, 845
- Behroozi P. S., Wechsler R. H., Lu Y., Hahn O., Busha M. T., Klypin A., Primack J. R., 2014, *The Astrophysical Journal*, 787, 156
- Berti A. M., Coil A. L., Behroozi P. S., Eisenstein D. J., Bray A. D., Cool R. J., Moustakas J., 2017, *The Astrophysical Journal*, 834, 87
- Blanton M. R., Roweis S., 2007, *The Astronomical Journal*, 133, 734

- Blanton M. R., et al., 2005, *The Astronomical Journal*, 129, 2562
- Bluck A. F. L., Maiolino R., Brownson S., Conselice C. J., Ellison S. L., Piotrowska J. M., Thorp M. D., 2022, *Astronomy and Astrophysics*, 659, A160
- Boquien M., Burgarella D., Roehly Y., Buat V., Ciesla L., Corre D., Inoue A. K., Salas H., 2019, *Astronomy and Astrophysics*, 622, A103
- Bray A. D., et al., 2016, *Monthly Notices of the Royal Astronomical Society*, 455, 185
- Bruzual G., Charlot S., 2003, *Monthly Notices of the Royal Astronomical Society*, 344, 1000
- Calderon V. F., Berlind A. A., Sinha M., 2018, *Monthly Notices of the Royal Astronomical Society*, 480, 2031
- Chabrier G., 2003, *Publications of the Astronomical Society of the Pacific*, 115, 763
- Cora S. A., et al., 2018, *Monthly Notices of the Royal Astronomical Society*, 479, 2
- Croton D. J., et al., 2006, *Monthly Notices of the Royal Astronomical Society*, 365, 11
- Davis M., Efstathiou G., Frenk C. S., White S. D. M., 1985, *The Astrophysical Journal*, 292, 371
- Davis B. L., Graham A. W., Cameron E., 2018, *The Astrophysical Journal*, 869, 113
- De Lucia G., Blaizot J., 2007, *Monthly Notices of the Royal Astronomical Society*, 375, 2
- Dekel A., Birnboim Y., 2006, *Monthly Notices of the Royal Astronomical Society*, 368, 2
- Donnari M., et al., 2019, *Monthly Notices of the Royal Astronomical Society*, 485, 4817
- Donnari M., Pillepich A., Nelson D., Marinacci F., Vogelsberger M., Hernquist L., 2021, *Monthly Notices of the Royal Astronomical Society*, p. stab1950
- Ellis S. C., Driver S. P., Allen P. D., Liske J., Bland-Hawthorn J., De Propris R., 2005, *Monthly Notices of the Royal Astronomical Society*, 363, 1257
- Fabian A. C., 2012, *Annual Review of Astronomy and Astrophysics*, 50, 455
- Fakhouri O., Ma C.-P., 2009, *Monthly Notices of the Royal Astronomical Society*, 394, 1825
- Gensior J., Kruijssen J. M. D., Keller B. W., 2020, *Monthly Notices of the Royal Astronomical Society*, 495, 199
- Genzel R., et al., 2014, *The Astrophysical Journal*, 785, 75
- Gunn J. E., Gott III J. R., 1972, *The Astrophysical Journal*, 176, 1
- Guo Q., et al., 2011, *Monthly Notices of the Royal Astronomical Society*, 413, 101
- Habouzit M., et al., 2021, *Monthly Notices of the Royal Astronomical Society*, 503, 1940
- Hartley W. G., Conselice C. J., Mortlock A., Foucaud S., Simpson C., 2015, *Monthly Notices of the Royal Astronomical Society*, 451, 1613
- Hearin A. P., Watson D. F., van den Bosch F. C., 2015, *Monthly Notices of the Royal Astronomical Society*, 452, 1958
- Hearin A. P., Behroozi P. S., van den Bosch F. C., 2016, *Monthly Notices of the Royal Astronomical Society*, 461, 2135
- Henriques B. M. B., White S. D. M., Thomas P. A., Angulo R., Guo Q., Lemson G., Springel V., Overzier R., 2015, *Monthly Notices of the Royal Astronomical Society*, 451, 2663
- Henriques B. M. B., Yates R. M., Fu J., Guo Q., Kauffmann G., Srisawat C., Thomas P. A., White S. D. M., 2020, *Monthly Notices of the Royal Astronomical Society*, 491, 5795
- Hogg D. W., et al., 2002, *The Astronomical Journal*, 124, 646
- Jian H.-Y., Lin L., Chiueh T., 2012, *The Astrophysical Journal*, 754, 26
- Kampeczyk P., et al., 2013, *The Astrophysical Journal*, 762, 43
- Kauffmann G., 2015, *Monthly Notices of the Royal Astronomical Society*, 454, 1840
- Kauffmann G., et al., 2003, *Monthly Notices of the Royal Astronomical Society*, 341, 33
- Kauffmann G., Li C., Zhang W., Weinmann S., 2013, *Monthly Notices of the Royal Astronomical Society*, 430, 1447
- Kawinwanichakij L., et al., 2016, *The Astrophysical Journal*, 817, 9
- Knobel C., Lilly S. J., Woo J., Kovač K., 2015, *The Astrophysical Journal*, 800, 24
- Kormendy J., Ho L. C., 2013, *Annual Review of Astronomy and Astrophysics*, 51, 511
- Kormendy J., Bender R., Cornell M. E., 2011, *Nature*, 469, 374
- Lacerna I., Contreras S., González R. E., Padilla N., Gonzalez-Perez V., 2018, *Monthly Notices of the Royal Astronomical Society*, 475, 1177
- Lacerna I., et al., 2022, *Monthly Notices of the Royal Astronomical Society*, 513, 2271
- Larson R. B., Tinsley B. M., Caldwell C. N., 1980, *The Astrophysical Journal*, 237, 692
- Li C., Kauffmann G., Jing Y. P., White S. D. M., Börner G., Cheng F. Z., 2006, *Monthly Notices of the Royal Astronomical Society*, 368, 21
- Li C., Wang L., Jing Y. P., 2013, *The Astrophysical Journal*, 762, L7
- Li Q., et al., 2022, *The Astrophysical Journal*, 933, 9
- Lim S. H., Mo H. J., Lu Y., Wang H., Yang X., 2017, *Monthly Notices of the Royal Astronomical Society*, 470, 2982
- Lintott C., et al., 2011, *Monthly Notices of the Royal Astronomical Society*, 410, 166
- Lu Y., et al., 2016, *The Astrophysical Journal*, 832, 1
- Magorrian J., et al., 1998, *The Astronomical Journal*, 115, 2285
- Mancera Piña P. E., Fraternali F., Oosterloo T., Adams E. A. K., di Teodoro E., Bacchini C., Iorio G., 2022, *Monthly Notices of the Royal Astronomical Society*, 514, 3329
- Mandelbaum R., Seljak U., Cool R. J., Blanton M., Hirata C. M., Brinkmann J., 2006, *Monthly Notices of the Royal Astronomical Society*, 372, 758
- Mandelbaum R., Wang W., Zu Y., White S., Henriques B., More S., 2016, *Monthly Notices of the Royal Astronomical Society*, 457, 3200
- Marinacci F., et al., 2018, *Monthly Notices of the Royal Astronomical Society*, 480, 5113
- Martig M., Bournaud F., Teyssier R., Dekel A., 2009, *The Astrophysical Journal*, 707, 250
- Mo H. J., White S. D. M., 1996, *Monthly Notices of the Royal Astronomical Society*, 282, 347
- Mo H., Van den Bosch F., White S., 2010, *Galaxy Formation and Evolution*. Cambridge University Press, Cambridge ; New York
- Moore B., Katz N., Lake G., Dressler A., Oemler A., 1996, *Nature*, 379, 613
- More S., van den Bosch F. C., Cacciato M., Skibba R., Mo H. J., Yang X., 2011, *Monthly Notices of the Royal Astronomical Society*, 410, 210
- Muldrew S. I., et al., 2012, *Monthly Notices of the Royal Astronomical Society*, 419, 2670
- Naiman J. P., et al., 2018, *Monthly Notices of the Royal Astronomical Society*, 477, 1206
- Nelson D., et al., 2018, *Monthly Notices of the Royal Astronomical Society*, 475, 624
- Nelson D., et al., 2019, *Computational Astrophysics and Cosmology*, 6, 2
- Noll S., Burgarella D., Giovannoli E., Buat V., Marcillac D., Muñoz-Mateos J. C., 2009, *Astronomy and Astrophysics*, 507, 1793
- Otter J. A., Masters K. L., Simmons B., Lintott C. J., 2020, *Monthly Notices of the Royal Astronomical Society*, 492, 2722
- Paranjape A., Kovač K., Hartley W. G., Pahwa I., 2015, *Monthly Notices of the Royal Astronomical Society*, 454, 3030
- Peng Y.-j., Renzini A., 2020, *Monthly Notices of the Royal Astronomical Society*, 491, L51
- Peng Y.-j., et al., 2010, *The Astrophysical Journal*, 721, 193
- Peng Y.-j., Lilly S. J., Renzini A., Carollo M., 2012, *The Astrophysical Journal*, 757, 4
- Peng Y., Maiolino R., Cochrane R., 2015, *Nature*, 521, 192
- Pillepich A., et al., 2018a, *Monthly Notices of the Royal Astronomical Society*, 473, 4077
- Pillepich A., et al., 2018b, *Monthly Notices of the Royal Astronomical Society*, 475, 648
- Piotrowska J. M., Bluck A. F. L., Maiolino R., Peng Y., 2022, *Monthly Notices of the Royal Astronomical Society*, 512, 1052
- Planck Collaboration et al., 2016, *Astronomy & Astrophysics*, 594, A13
- Poole G. B., Mutch S. J., Croton D. J., Wyithe S., 2017, *Monthly Notices of the Royal Astronomical Society*, 472, 3659
- Posti L., Fall S. M., 2021, *Astronomy and Astrophysics*, 649, A119

- Posti L., Fraternali F., Marasco A., 2019, *Astronomy and Astrophysics*, 626, A56
- Pozzetti L., et al., 2010, *Astronomy & Astrophysics*, 523, A13
- Renzini A., 2020, *Monthly Notices of the Royal Astronomical Society*, 495, L42
- Rodriguez-Gomez V., et al., 2015, *Monthly Notices of the Royal Astronomical Society*, 449, 49
- Salim S., et al., 2016, *The Astrophysical Journal Supplement Series*, 227, 2
- Salim S., Boquien M., Lee J. C., 2018, *The Astrophysical Journal*, 859, 11
- Shi J., et al., 2022, *The Astrophysical Journal*, 927, 189
- Sin L. P. T., Lilly S. J., Henriques B. M. B., 2017, *Monthly Notices of the Royal Astronomical Society*, 471, 1192
- Sin L. P. T., Lilly S. J., Henriques B. M. B., 2019, *Monthly Notices of the Royal Astronomical Society*, 488, 234
- Smith R., Davies J. I., Nelson A. H., 2010, *Monthly Notices of the Royal Astronomical Society*, 405, 1723
- Springel V., 2010, *Monthly Notices of the Royal Astronomical Society*, 401, 791
- Springel V., White S. D. M., Tormen G., Kauffmann G., 2001, *Monthly Notices of the Royal Astronomical Society*, 328, 726
- Springel V., et al., 2018, *Monthly Notices of the Royal Astronomical Society*, 475, 676
- Strateva I., et al., 2001, *The Astronomical Journal*, 122, 1861
- Sun S., Guo Q., Wang L., Lacey C. G., Wang J., Gao L., Pan J., 2018, *Monthly Notices of the Royal Astronomical Society*, 477, 3136
- Terrazas B. A., et al., 2020, *Monthly Notices of the Royal Astronomical Society*, 493, 1888
- Tinker J. L., Wetzel A. R., Conroy C., Mao Y.-Y., 2017, *Monthly Notices of the Royal Astronomical Society*, 472, 2504
- Tinker J. L., Hahn C., Mao Y.-Y., Wetzel A. R., Conroy C., 2018a, *Monthly Notices of the Royal Astronomical Society*, 477, 935
- Tinker J. L., Hahn C., Mao Y.-Y., Wetzel A. R., 2018b, *Monthly Notices of the Royal Astronomical Society*, 478, 4487
- Treyer M., et al., 2018, *Monthly Notices of the Royal Astronomical Society*, 477, 2684
- Wang H., Mo H. J., Jing Y. P., 2009, *Monthly Notices of the Royal Astronomical Society*, 396, 2249
- Wang J., et al., 2015, *Monthly Notices of the Royal Astronomical Society*, 453, 2399
- Wang L., Li C., Jing Y. P., 2016, *The Astrophysical Journal*, 819, 58
- Wang H., et al., 2018, *The Astrophysical Journal*, 852, 31
- Wang K., Mo H. J., Li C., Meng J., Chen Y., 2020, *Monthly Notices of the Royal Astronomical Society*, 499, 89
- Wang K., Chen Y., Li Q., Yang X., 2023a, *arXiv e-prints*, p. [arXiv:2304.07189](https://arxiv.org/abs/2304.07189)
- Wang K., Mo H., Li C., Chen Y., 2023b, *Monthly Notices of the Royal Astronomical Society*, 520, 1774
- Weinmann S. M., Van Den Bosch F. C., Yang X., Mo H. J., 2006, *Monthly Notices of the Royal Astronomical Society*, 366, 2
- Wetzel A. R., Tinker J. L., Conroy C., van den Bosch F. C., 2014, *Monthly Notices of the Royal Astronomical Society*, 439, 2687
- Woo J., et al., 2013, *Monthly Notices of the Royal Astronomical Society*, 428, 3306
- Xu B., Peng Y., 2021, *The Astrophysical Journal Letters*, 923, L29
- Yang X., Mo H. J., van den Bosch F. C., Jing Y. P., 2005, *Monthly Notices of the Royal Astronomical Society*, 356, 1293
- Yang X., Mo H. J., van den Bosch F. C., Pasquali A., Li C., Barden M., 2007, *The Astrophysical Journal*, 671, 153
- Yang X., et al., 2021, *The Astrophysical Journal*, 909, 143
- York D. G., et al., 2000, *The Astronomical Journal*, 120, 1579
- Zhang Z., et al., 2021a, *Astronomy and Astrophysics*, 650, A155
- Zhang C., et al., 2021b, *The Astrophysical Journal*, 911, 57
- Zhang Z., Wang H., Luo W., Zhang J., Mo H. J., Jing Y., Yang X., Li H., 2022, *Astronomy and Astrophysics*, 663, A85
- Zu Y., Mandelbaum R., 2018, *Monthly Notices of the Royal Astronomical Society*, 476, 1637

This paper has been typeset from a $\text{\TeX}/\text{\LaTeX}$ file prepared by the author.